IOPscience iopscience.iop.org

Home Search Collections Journals About Contact us My IOPscience

Carbon cycle and climate effects of forcing from fire-emitted aerosols

This content has been downloaded from IOPscience. Please scroll down to see the full text.

2017 Environ. Res. Lett. 12 025002

(http://iopscience.iop.org/1748-9326/12/2/025002)

View the table of contents for this issue, or go to the journal homepage for more

Download details:

IP Address: 210.77.64.106
This content was downloaded on 30/03/2017 at 11:17

Please note that terms and conditions apply.

You may also be interested in:

Why must a solar forcing be larger than a CO2 forcing to cause the same global mean surface temperature change?
Angshuman Modak, Govindasamy Bala, Long Cao et al.

A framework to understand the transient climate response to emissions
Richard G Williams, Philip Goodwin, Vassil M Roussenov et al.

The effectiveness of net negative carbon dioxide emissions in reversing anthropogenic climate change
Katarzyna B Tokarska and Kirsten Zickfeld

Assessing the implications of human land-use change for the transient climate response to cumulative carbon emissions
C T Simmons and H D Matthews

Enhanced Australian carbon sink despite increased wildfire during the 21st century
D I Kelley and S P Harrison

The first-order effect of Holocene Northern Peatlands on global carbon cycle dynamics
Yi Wang, Nigel T Roulet, Steve Frolking et al.

Examination of a climate stabilization pathway via zero-emissions using Earth system models
Daisuke Nohara, J Tsutsui, S Watanabe et al.

Ecosystem responses to recent climate change and fire disturbance at northern highlatitudes: observations and model results contrasting northern Eurasia and NorthAmerica
S J Goetz, M C Mack, K R Gurney et al.

Environmental Research Letters

LETTER

Carbon cycle and climate effects of forcing from fire-emitted aerosols

Jean-Sébastien Landry[1,3], Antti-Ilari Partanen[1,2] and H Damon Matthews[1]

[1] Department of Geography, Planning and Environment, Concordia University, 1455 boul. de Maisonneuve Ouest, Montréal, Québec, H3G 1M8, Canada
[2] Climate Change, Finnish Meteorological Institute, P.O. Box 503, Helsinki, 00101, Finland
[3] Currently at the Département de géomatique appliquée, Université de Sherbrooke, 2500 boul. de l'Université, Sherbrooke, Québec, J1K 2R1, Canada

E-mail: jean-sebastien.landry@usherbrooke.ca

OPEN ACCESS

RECEIVED
14 June 2016

REVISED
16 November 2016

ACCEPTED FOR PUBLICATION
6 December 2016

PUBLISHED
25 January 2017

Keywords: aerosols, fire, carbon cycle, modelling, remote effects, feedbacks

Supplementary material for this article is available online

Original content from this work may be used under the terms of the Creative Commons Attribution 3.0 licence.

Any further distribution of this work must maintain attribution to the author(s) and the title of the work, journal citation and DOI.

Abstract

Aerosols emitted by landscape fires affect many climatic processes. Here, we combined an aerosol–climate model and a coupled climate–carbon model to study the carbon cycle and climate effects caused by fire-emitted aerosols (FEA) forcing at the top of the atmosphere and at the surface. This forcing ('best guess' present-day values of −0.10 and −1.3 W m^{-2} at the top of the atmosphere and surface, respectively) had a predominant cooling influence that altered regional land carbon stocks on decadal timescales by modifying vegetation productivity and soil–litter decomposition. Changes in regional land and ocean carbon stocks became much stronger for FEA forcing acting on multi-century timescales; this occurred because carbon stocks responded to the forcing itself on such timescales and also due to gradual effects on the climate (e.g. through increased sea ice cover) that further affected the carbon cycle. Carbon increases and decreases in different regions partly offset each other, so that absolute changes in global land, atmosphere, and ocean stocks were all <2 Pg C after 30 years of FEA forcing and <6 Pg C after more than 1000 years of FEA forcing. FEA-caused changes in land carbon storage did not substantially modify the magnitude of FEA emissions, suggesting there is no consequential regional-scale positive feedback loop between these two elements. However, we found indications that the FEA-caused cooling from frequently-burning regions in Africa and Australia increased land carbon stocks in eastern South America and equatorial Asia, respectively. This suggests the potential for remote carbon cycle effects from regions emitting large amounts of fire aerosols.

1. Introduction

Aerosols emitted during landscape fire events lead to a suite of impacts in the Earth system. By decreasing air quality, fire-emitted aerosols (FEA) could result in ~300000 deaths annually (Johnston *et al* 2012). FEA also directly affect radiation exchanges throughout the atmosphere and modify cloud properties, generally decreasing precipitation and reducing surface radiation (Jones *et al* 2007, Jacobson 2014, Veira *et al* 2015, Jiang *et al* 2016). The net radiative forcing caused by FEA is highly uncertain, but might determine whether fires have a net warming or cooling influence on global climate (Jacobson 2004, Unger *et al* 2010, Ward *et al* 2012, Jacobson 2014, Landry *et al* 2015).

FEA also modify carbon cycling through changes in nutrient distribution and physical climate (Mahowald 2011, Mahowald *et al* 2011). Nutrient-mediated effects happen as fires redistribute nitrogen and phosphorus (Mahowald *et al* 2005, Chen *et al* 2010) and fertilize oceans through iron deposition, although this last mechanism is likely consequential at the regional scale only (Guieu *et al* 2005). Effects mediated through changes in physical climate include the FEA-caused increase in diffuse radiation that

© 2017 IOP Publishing Ltd

enhances vegetation productivity (Rap *et al* 2015) and net ecosystem carbon uptake (Doughty *et al* 2010); this last study also found that FEA-caused cooling can enhance net ecosystem carbon uptake. In a previous study using a simplified approach to account for the FEA-caused radiative forcing at the top of the atmosphere and resulting temperature changes (but that neglected surface radiation changes), we reported that a very strong FEA-caused cooling could substantially increase land carbon storage by slowing down soil–litter decomposition, to the point where more frequent fires actually increased global land carbon stocks for many decades (Landry *et al* 2015). This outcome suggests the possibility of a strong regional-scale positive feedback between FEA forcing and carbon stocks, such that FEA-induced cooling from a given fire regime would increase land carbon storage, thereby increasing fuel stocks, leading to higher FEA amounts, and resulting in more cooling and land carbon storage.

Here, we combined an aerosol–climate model and a coupled climate–carbon model to study the impacts on carbon cycling due to FEA-caused changes in the physical climate, more precisely the modification of shortwave and longwave radiation fluxes at the top of the atmosphere (i.e. the effective radiative forcing (ERF); Myhre *et al* 2013) as well as shortwave radiation at the surface. To our knowledge, this is the first study assessing FEA effects on the carbon cycle in a global climate model. The main objective was to quantify FEA-caused changes in land, atmosphere, and ocean carbon stocks. We also considered various sources of uncertainty to provide insights about modelling FEA effects on the carbon cycle.

2. Methods

2.1. Coupled climate–carbon model

The University of Victoria Earth System Climate Model (UVic ESCM) version 2.9 is a coupled climate–carbon model of intermediate complexity simulating the exchanges of carbon, energy, and water among land, atmosphere, and ocean (Weaver *et al* 2001, Eby *et al* 2009). Atmospheric processes are represented through simplified energy and moisture balance equations with dynamical feedbacks (Weaver *et al* 2001). The ocean module simulates three-dimensional circulation, sea ice dynamics and thermodynamics, inorganic carbon cycling, and ecosystem/biogeochemical carbon–nutrient dynamics (Weaver *et al* 2001, Ewen *et al* 2004, Schmittner *et al* 2008, Eby *et al* 2009). Terrestrial processes are represented with a simplified land surface scheme (Meissner *et al* 2003) coupled to a dynamic global vegetation model (Cox 2001) that accounts for competition among five plant functional types (PFTs) as well as carbon stocks in vegetation and soil–litter. Each month, fire-caused emissions were computed as the product of prescribed burned area, PFT-specific fuel density simulated by the UVic ESCM, and PFT-specific combustion fractions; vegetation killed by fire but not fully combusted joined soil–litter, where it decomposed as a function of the local soil temperature and moisture that were influenced by fire-caused changes in atmospheric CO_2 and surface albedo (Landry *et al* 2015, Landry and Matthews 2016). We used the same prescribed burned area as Landry *et al* (2015), i.e. monthly-varying mean values for 2001–2012 from version 4 of the Global Fire Emissions Database (GFED4) (Giglio *et al* 2013). PFTs could colonize the burned area after each fire event, leading to a CO_2 regrowth flux that depended upon local competition among PFTs and was also influenced by fire-caused changes in the climate–carbon system. This approach captured the impacts of fire from local (e.g. altered vegetation composition) to global (e.g. fire-caused CO_2 fertilization) scales as well as the carbon trade-offs between fire and land-cover changes (i.e. fire-caused decreases in biomass density led to smaller carbon emissions from land-cover changes; Ward *et al* 2012). However, the UVic ESCM did not account for the increase in diffuse radiation that has been studied elsewhere (Doughty *et al* 2010, Rap *et al* 2015) or for the impacts of nutrient redistribution (Guieu *et al* 2005, Mahowald *et al* 2005, Chen *et al* 2010). We also neglected year-to-year variability in fire regime because we focussed on mean effects over decadal to multi-century timescales. Since we wanted to isolate FEA effects, we activated the fire module in all simulations but neglected FEA-caused forcing in the control simulations.

2.2. Amounts of fire-emitted aerosols

Here, we added to the UVic ESCM the computation of black carbon (BC), organic carbon (OC), and sulphur dioxide (SO_2, a precursor of sulphate aerosols) emissions. We derived the required emission factors by combining GFED4 values (GFED4 2014), themselves based on Andreae and Merlet (2001) and Akagi *et al* (2011), with a conversion factor of 0.48 kg C per kg of dry matter (van der Werf *et al* 2010). With these emission factors, simulation TR-30-MIN (see section 2.4) gave 2001–2012 mean global emissions (in Tg species/year) of 1.9 for BC, 15.5 for OC, and 2.2 for SO_2, all within 6% of the GFED4 results (GFED4 2014). When compared to satellite, surface, and airborne observations, such results appear underestimated and have often been scaled up (Johnston *et al* 2012, Kaiser *et al* 2012, Ward *et al* 2012, Tosca *et al* 2013, Rap *et al* 2015). We therefore used three sets of FEA. We took the values derived from GFED4 emission factors as the minimum (MIN) estimates. For the maximum (MAX) estimates, we scaled the previous emissions by a factor of 5 (Johnston *et al*

Table 1. List of UVic ESCM simulations with associated FEA forcing from ECHAM-HAMMOZ.

	UVic ESCM				ECHAM-HAMMOZ		
Name[a]	Start	Period	Length	FEA forcing	FEA input[b]	Non-FEA[c]	Meteorology
TR-CONT	1850	1851–2020	170 yr	None	–	–	–
EQ-CONT	1850	1850	1000 yr	None	–	–	–
TR-30-X	1850	1851–2020	170 yr	1991–2020	TR-CONT	2005	2002–2008
EQ-1000-X	1850	1850	1000 yr	Always	EQ-CONT	1850	2002–2008
TR-1170-X	EQ-1000-X	1851–2020	170 yr	Always	TR-CONT	2005	2002–2008
TR-30-X-M	1850	1851–2020	170 yr	1991–2020	TR-CONT	2005	1992–1998
TR-1170-X-F	EQ-1000-X	1851–2020	170 yr	Always	TR-1170-X	2005	2002–2008

[a] X is for the FEA amount (MIN, BG, or MAX);
[b] FEA input to ECHAM-HAMMOZ from the last 30 years of the UVic ESCM simulation, except for EQ-CONT (last 50 years);
[c] emission year for aerosols other than FEA.

2012, Tosca *et al* 2013, Rap *et al* 2015). For the best guess (BG) estimates, we used a two-step procedure. First, we computed the mean scaling factors from previous studies (Johnston *et al* 2012, Ward *et al* 2012, Tosca *et al* 2013) across the 14 GFED regions. Second, we adjusted all these regional emission factors so that the global emissions were three (for BC and OC) and two (for SO_2) times higher than the MIN estimates (Johnston *et al* 2012, Kaiser *et al* 2012, Ward *et al* 2012, Tosca *et al* 2013).

2.3. Forcing from fire-emitted aerosols

The simplified atmospheric module of the UVic ESCM makes long simulations computationally affordable, but prevents the process-based representation of FEA effects. To calculate the ERF and modified surface radiation caused by FEA, we used the ECHAM-HAMMOZ (ECHAM6.1-HAM2) aerosol–climate model (Zhang *et al* 2012, Stevens *et al* 2013). The model core is the atmospheric general circulation model ECHAM, which solves atmospheric flow and physics at a horizontal resolution of T63 (roughly $1.9° \times 1.9°$). The aerosol model HAM explicitly simulates emissions, microphysics, and removal of aerosol particles. Aerosol–cloud interactions are calculated online (Lohmann *et al* 2007) with the Lin and Leaitch (1997) semi-empirical cloud activation scheme (Lohmann *et al* 1999). The model accounts for aerosol direct, semi-direct, and indirect effects. BC, OC, and SO_2 from fire were distributed vertically based on predefined rules (Dentener *et al* 2006). We nudged ECHAM-HAMMOZ meteorology towards ERA-Interim reanalysis data (Dee *et al* 2011) and prescribed sea surface temperature. The runs lasted six years, in addition to the one-year spin-up period; similarly to FEA, emissions of anthropogenic aerosols did not vary between years. We performed all ECHAM-HAMMOZ simulations with and without monthly-varying FEA to diagnose the FEA-caused forcing. The resulting monthly-varying forcing fields then served as input data to modify radiation exchanges in the UVic ESCM at the top of the atmosphere and at the surface.

2.4. Simulation design

We performed transient (TR) and equilibrium (EQ) control simulations (CONT) in the UVic ESCM with the fire module, but without FEA forcing (table 1). These simulations started from previous results (Landry *et al* 2015) for year 1850 that included prescribed natural and anthropogenic forcings as well as the effect of fire. TR-CONT was driven by prescribed transient forcings during the 1851–2020 period simulated here, whereas EQ-CONT lasted 1000 years with prescribed forcings kept at their year-1850 values. Prescribed forcings in the UVic ESCM consisted of anthropogenic CO_2 emissions, other greenhouse gases, sulphate and volcanic aerosols, land-cover changes, and land ice (Weaver *et al* 2001, Matthews *et al* 2004). Forcings came from historical data for 1850–2005 (Eby *et al* 2013) and the Representative Concentration Pathway (RCP) 4.5 for 2006–2020 (van Vuuren *et al* 2011).

TR-30-X was similar to TR-CONT but included the effect of FEA forcing in the UVic ESCM during the 30-year period from 1991 to 2020; here X stands for the amount of FEA (MIN, BG, or MAX) calculated from the last 30 years of TR-CONT. FEA forcing was computed by ECHAM-HAMMOZ based on this UVic ESCM-estimated FEA amount, year-2005 emissions for aerosols other than FEA, and 2002–2008 meteorology. In all simulations, the non-aerosol forcings required by ECHAM-HAMMOZ (e.g. ozone concentration) were for year 2005. EQ-1000-X was similar to EQ-CONT but included the effect of FEA forcing for 1000 years, computed by ECHAM-HAMMOZ based on UVic ESCM-estimated FEA amount over the last 50 years of EQ-CONT, year-1850 emissions for aerosols other than FEA, and 2002–2008 meteorology. We used EQ-1000-X results as the starting point for TR-1170-X. This transient simulation included the same FEA forcing as TR-30-X, but applied from 1851 until 2020. Including the 1000-year EQ-1000-X equilibrium, TR-1170-X therefore felt FEA forcing over a total of 1170 years, with a switch from preindustrial to present-day FEA forcing on year 1851. We also performed sensitivity

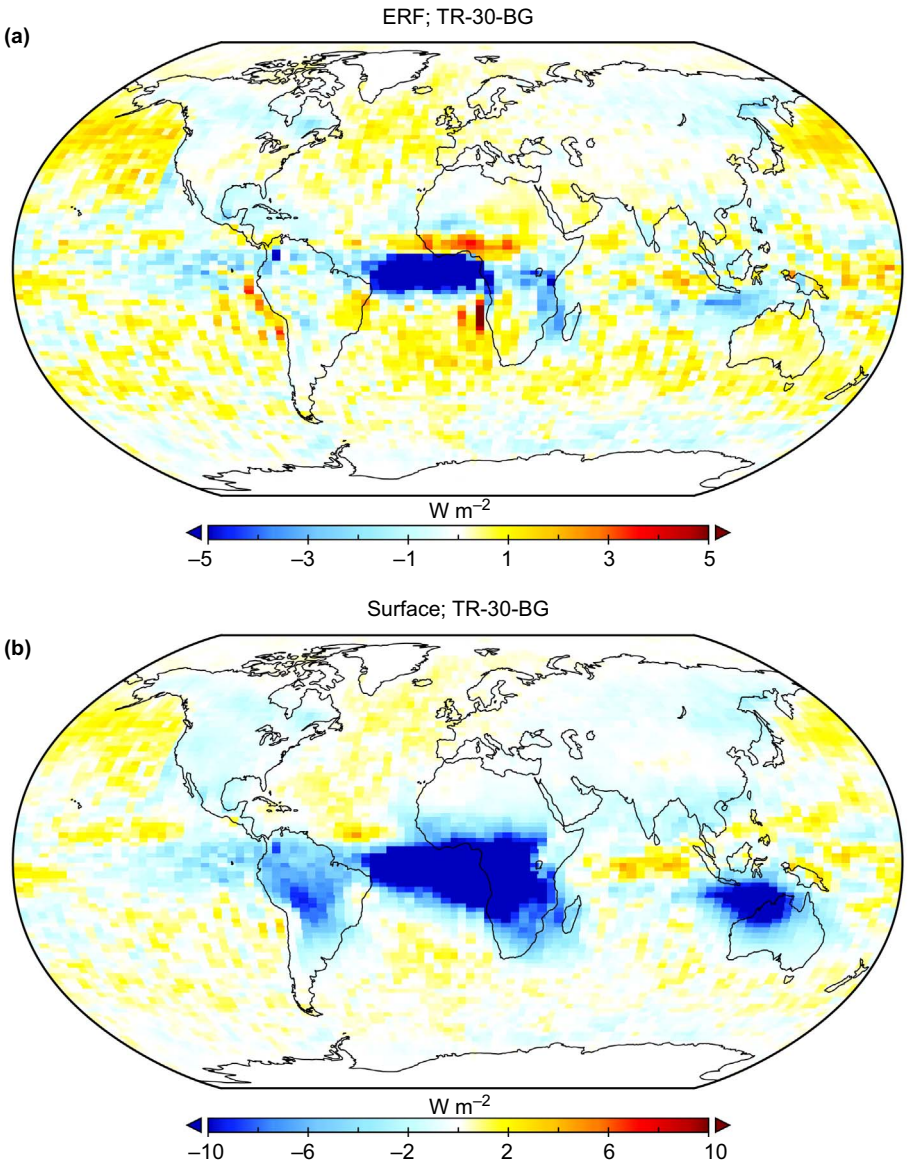

Figure 1. Total (shortwave and longwave) effective radiative forcing (a) and difference in shortwave surface radiation (b) caused by fire-emitted aerosols in ECHAM-HAMMOZ over 1991–2020 for the best guess estimate of fire-emitted aerosols amount (simulation TR-30-BG). Results are annual mean values, in W m^{-2}.

simulations. TR-30-X-M was similar to TR-30-X, except that ECHAM-HAMMOZ was nudged towards the 1992–1998 meteorology instead of 2002–2008. TR-1170-X-F was similar to TR-1170-X, except that the UVic ESCM-estimated FEA magnitude used by ECHAM-HAMMOZ came from TR-1170-X instead of TR-CONT. The purpose here was to assess potential feedbacks between FEA and the carbon cycle by comparing results for FEA magnitudes that themselves felt (TR-1170-X-F) or not (TR-1170-X) the long-term influence of FEA forcing.

Unless otherwise mentioned, results correspond to the difference between a simulation with FEA forcing and the corresponding control (TR-CONT or EQ-CONT), thereby isolating FEA effects. We also note that even if MIN, BG, and MAX results actually came from different FEA amounts in ECHAM-HAMMOZ, the range of values presented below assesses the results sensitivity to varying FEA forcing strengths as estimated by other aerosol–climate models.

3. Results

3.1. Effects for 30-year forcing

Figure 1 shows FEA-caused ERF and surface radiation changes for TR-30-BG. The strongest negative ERF values occurred west of central Africa, whereas extensive regions of predominantly positive ERF were centered over the northern Pacific and around Australia. FEA usually decreased surface radiation, above all in the vicinity of Africa and Australia, i.e. the regions with the highest fire frequency. Spatial patterns were similar for MIN and MAX (figure S1), with weaker forcing for MIN and stronger forcing for MAX. Global mean ERF was −0.10, −0.03, and −0.25 W m^{-2} for BG, MIN, and MAX, respectively.

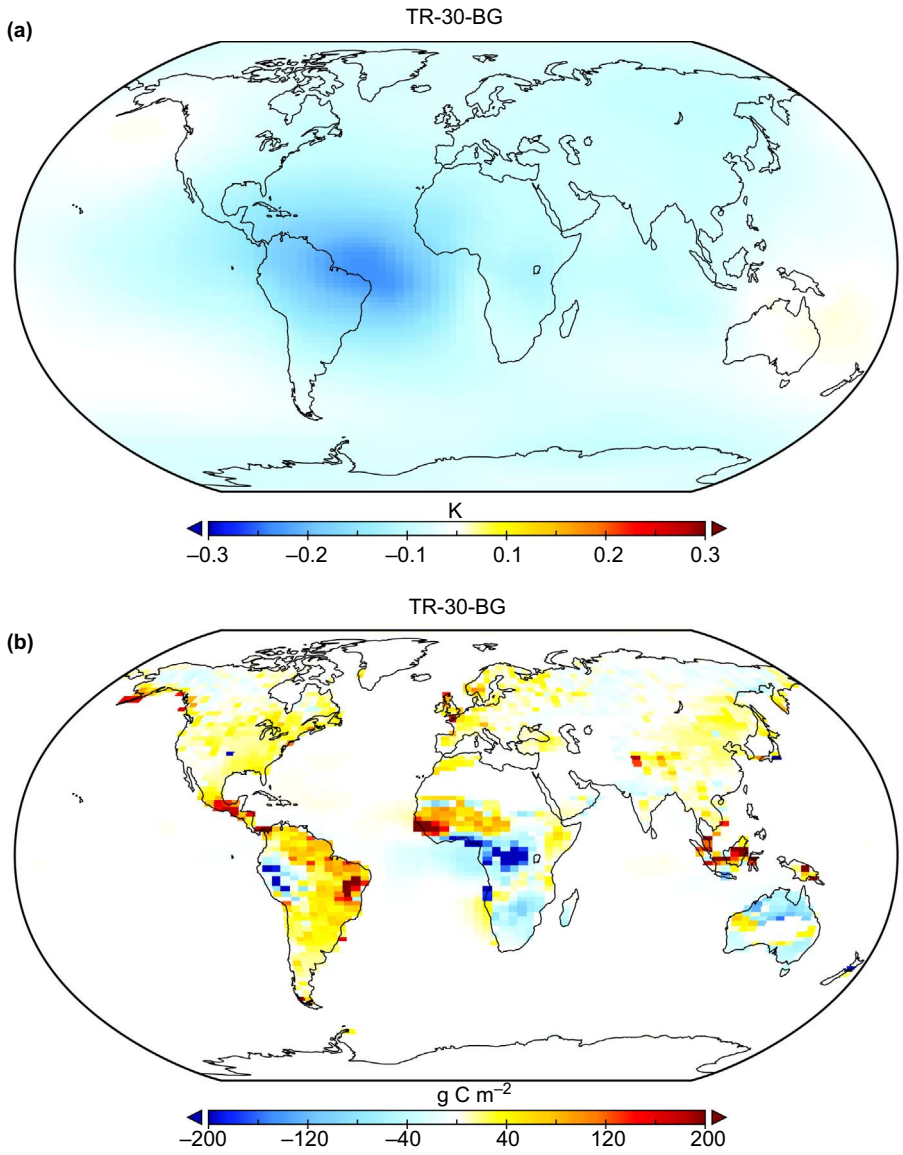

Figure 2. Mean effect of 30-year forcing on atmospheric surface temperature (a, in K) and carbon stocks (b, in g C m^{-2}) in the UVic ESCM over 1991–2020 for the best guess estimate of fire-emitted aerosols amount (simulation TR-30-BG). Land results include vegetation and soil–litter, and ocean results are the column-integrated values per unit of surface area.

BG and MAX results were similar to the −0.1 to −0.3 W m^{-2} range from previous studies that also accounted for aerosol–cloud interactions (Jones *et al* 2007, Unger *et al* 2010, Rap *et al* 2013, Veira *et al* 2015), although positive (Jacobson 2014) and substantially more negative (Jacobson 2004, Ward *et al* 2012, Jiang *et al* 2016) values have also been reported. The global mean change in surface radiation was −1.3, −0.4, and −2.3 W m^{-2} for BG, MIN, and MAX, respectively. BG and MAX were comparable to previous studies (Jones *et al* 2007, Veira *et al* 2015, Jiang *et al* 2016).

The different meteorology had a small impact on simulated forcing. Spatial patterns were very similar although some differences were visible, especially for ERF (e.g. figures 1 vs. S2 for BG). The impact of meteorology on global mean ERF (a difference of 0.05 W m^{-2} between TR-30-BG-M and TR-30-BG) was also much smaller than the uncertainty associated with different FEA amounts (a difference of 0.22 W m^{-2} between TR-30-MIN and TR-30-MAX). Consequently, we henceforth present results for the 2002–2008 meteorology only.

When applied over 30 years (1991–2020) in the UVic ESCM, the BG forcing from ECHAM-HAMMOZ generally decreased atmospheric surface temperature except around the Bering Strait and close to Australia (figure 2(*a*)). Changes in atmospheric surface temperature came not only from FEA-caused modifications to atmospheric radiation absorption, but also from FEA impacts on land and ocean surface conditions as well as from energy redistribution. The strongest cooling was located west of the strongest negative ERF (figure 1 (*a*)) due to prevailing westward winds at these latitudes. Similar results were obtained for MIN albeit with less cooling or more warming, whereas

Table 2. Changes in global carbon stocks in the UVic ESCM caused by the forcing from fire-emitted aerosols. Results (in Pg C) are mean values over 1991–2020.

Simulation	Land	Atmosphere	Ocean
30-year forcing from fire-emitted aerosols			
TR-30-BG	+1.1	−0.9	−0.2
TR-30-MIN	+1.4	−1.1	−0.3
TR-30-MAX	+1.6	−1.4	−0.2
1170-year forcing from fire-emitted aerosols			
TR-1170-BG	+2.3	−2.3	+0.2
TR-1170-MIN	+3.1	−1.0	−2.0
TR-1170-MAX	+0.6	−5.4	+5.0

more negative ERF for MAX led to cooling almost everywhere (figures S3(*a*) and S3(*c*)).

Changes in both temperature and surface radiation modified carbon stocks (figure 2(*b*)). The slight decrease in column-integrated ocean carbon west of central Africa involved lateral exchanges of carbon, because the colder surface temperature in this region actually increased the solubility of atmospheric CO_2. FEA usually increased land carbon, especially for most of Latin America, westernmost Africa, and equatorial Asia, but extensive decreases occurred in central Africa and northern Australia. FEA-induced cooling invariably slowed down soil–litter decomposition, yet soil–litter carbon decreased despite cooling in central Africa because the much lower surface radiation substantially reduced vegetation productivity, strongly decreasing the vegetation carbon input to the soil–litter pool. Conversely, vegetation productivity increased in some regions (e.g. westernmost Africa) despite lower surface radiation, due to the beneficial impact of FEA-caused cooling in warm climates (Steiner and Chameides 2005, Matthews *et al* 2007). Results for MIN and MAX were broadly similar to BG, with generally weaker and stronger effects, respectively (figures S3(*b*) and S3(*d*)).

At the local scale, changes in land carbon caused by 30-year FEA forcing often reached 1–3 % of total stocks, particularly in tropical regions. Yet changes in global carbon stocks were small (table 2). The first-order impact of FEA forcing was to increase global land carbon, which decreased atmospheric carbon. Ocean carbon stocks were also reduced, because the global decrease in atmospheric carbon had a larger effect than the overall cooling-related increase of CO_2 solubility. The effects on global carbon stocks were stronger for MIN than for BG, which resulted from opposite impacts of FEA on vegetation productivity vs. soil–litter decomposition at the global scale. For BG, reduced productivity due to lower surface radiation initially had more impact than reduced decomposition due to lower temperature, so that five years elapsed before FEA actually increased land carbon. For MIN, on the contrary, the change in global productivity was marginal and FEA immediately started augmenting land carbon.

3.2. Effects for forcing over a multi-century timescale

For simulations over many centuries, we first computed year-1850 FEA forcing. Results (figure S4) were broadly similar to the previous ones (figures 1 and S1), except that ERF and surface values were often slightly more negative in 1850 because lower anthropogenic aerosol levels led to stronger FEA-caused cloud-mediated effects (Spracklen and Rap 2013). We then performed a 1000-year equilibrium simulation in the UVic ESCM, with FEA forcing, for year 1850. When acting over such a long period, FEA-caused negative ERF triggered gradual changes in the physical state of the climate system, such as increased sea ice cover. As a result, for BG the global mean atmospheric surface temperature decreased by 0.11 K over the first 50 years, followed by an additional decrease of 0.07 K over the remaining 950 years (figure 3(*a*)). Responses were qualitatively similar for MIN and MAX, but noticeably less and more pronounced, respectively (figures S5(*a*) and S6(*a*)).

Starting from these year-1850 results, we performed a 1851–2020 transient simulation with the present-day FEA forcing used in section 3.1 applied throughout. The sudden decrease in the magnitude of negative ERF caused the warming impact visible around year 1850 in figure 3(*a*). At the end of the transient simulation, the change in atmospheric surface temperature for BG (figure 3(*b*)) was more negative than after applying FEA forcing over 30 years only (figure 2(*a*)), above all for the northern hemisphere due to increased Arctic sea ice cover. Effects were qualitatively similar for MIN (figures S5 (*b*) vs. S3(*a*)) and MAX (figures S6(*b*) vs. S3(*c*)).

Changes in 1991–2020 carbon stocks were clearly stronger for 1170-year (figure 3(*c*)) than for 30-year (figure 2(*b*)) FEA forcing. The stark contrast in ocean carbon changes between the Atlantic and Pacific broadly reflected the spatial differences in FEA-caused temperature changes, with ocean circulation contributing to finer-scale spatial patterns. Changes in land carbon often represented 1%–5% of local stocks. Land carbon changes for 1170-year vs. 30-year FEA forcing differed noticeably in boreal forests due to a legacy effect from the year-1850 equilibrium. At that time, FEA caused more negative ERF and much lower surface radiation over boreal forests than for present-day atmospheric conditions (figures S4(*a*)–(*b*) vs. 1(*a*)-–(*b*)). Moreover, the gradual increase of Arctic sea ice cover further decreased temperature in boreal forests. FEA therefore markedly reduced preindustrial boreal forests productivity, which decreased soil–litter stocks. A similar legacy effect was visible in the MIN results (figures S5(*c*) vs. S3(*b*)). For MAX, FEA forcing over both 1170-year and 30-year timescales generally reduced carbon stocks in boreal forests, but the decrease was larger in the former case (figures S6(*c*) vs. S3(*d*)).

Despite much stronger FEA impacts on local carbon stocks for 1170-year vs. 30-year forcing, the effects on global carbon stocks remained small

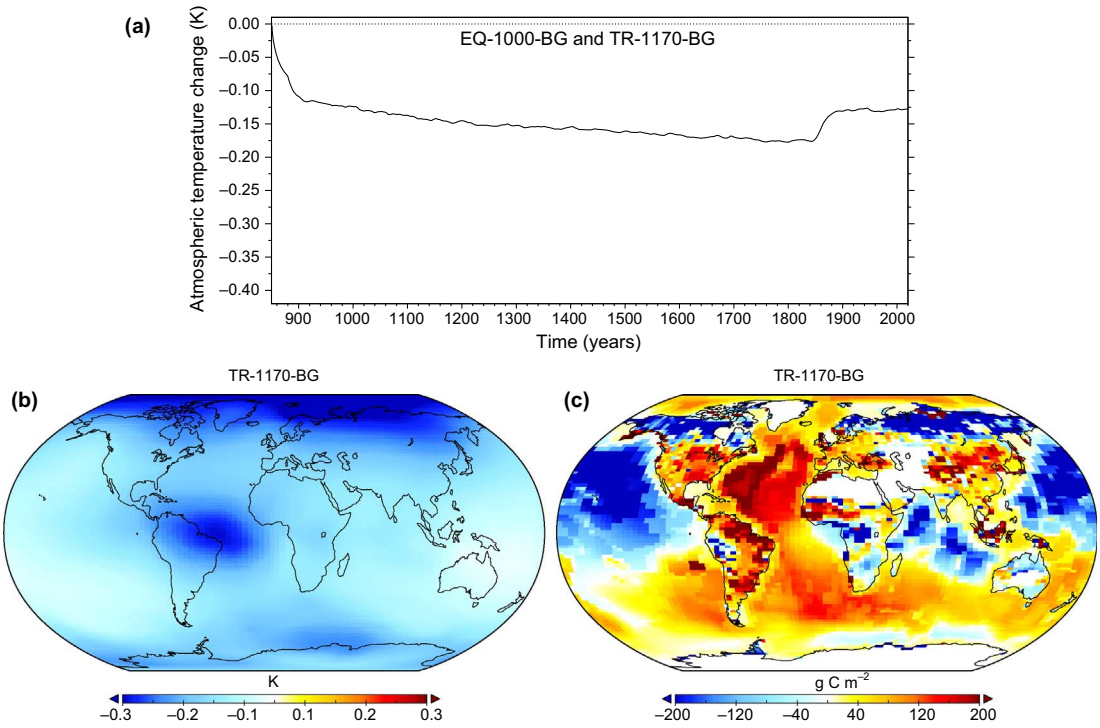

Figure 3. Effects of 1170-year forcing in the UVic ESCM for the best guess estimate of fire-emitted aerosols amount (simulations EQ-1000-BG and TR-1170-BG). (*a*) Transient effect on global mean atmospheric surface temperature (30-year running mean, in K); results for years 851–1850 are from EQ-1000-BG and results for years 1851–2020 are from TR-1170-BG. (*b*) Mean effect on atmospheric surface temperature (in K) over 1991–2020 for TR-1170-BG. (*c*) Mean effect on carbon stocks (in g C m^{-2}) over 1991–2020 for TR-1170-BG.

(table 2). The ordering of mean 1991–2020 land carbon increases (MIN > BG > MAX) came from the differences in FEA-caused changes between vegetation productivity and soil–litter decomposition rate. Changes in global atmospheric carbon were reversed compared to what they would have been based on land increases only (i.e. the smallest decrease for MIN and the largest decrease for MAX). This reflected the differences in enhanced CO_2 solubility due to FEA-caused cooling; for example, the large cooling for MAX led to net oceanic carbon uptake even though atmospheric CO_2 decreased.

Finally, we performed the TR-1170-X-F simulations to assess the potential for FEA-induced cooling to result in a positive feedback by enhancing land carbon storage and the magnitude of FEA produced. Local-scale land carbon changes were often affected by FEA–carbon cycle interactions (figure S7; results are for TR-1170-X-F minus TR-1170-X). For MAX, the effect led to higher global land carbon stocks (by 0.7 Pg C for TR-1170-MAX-F vs. TR-1170-MAX) and caused noticeable increases in regions where FEA already substantially augmented land carbon (e.g. eastern South America and westernmost Africa; figures S7(*c*) and S6(*c*)), suggestive of a possible positive feedback loop. Nonetheless, the overall potential for strong regional-scale positive FEA–carbon cycle feedbacks appeared small because: (1) the effect was spatially heterogeneous; (2) there was no large region where the effect showed a noticeable and invariable increase from MIN through BG to MAX, contrary to what one would expect for a positive feedback; and (3) for MIN and BG, total land carbon was lower (by ∼0.4 Pg C) for the TR-1170-X-F simulations.

4. Discussion

4.1. Effects of fire-emitted aerosols on the carbon cycle

We found that FEA-caused changes in both temperature and surface radiation affected carbon cycling. Over land, FEA decreased surface radiation almost everywhere and generally caused cooling. Lower surface radiation reduced vegetation productivity, but cooling had more variable impacts, for example increasing productivity in some tropical regions but decreasing it in cold climates. Changes in productivity altered input to soil–litter, which decomposed more slowly due to FEA-caused cooling. Local changes in land carbon therefore came from the complex interplay among several FEA-induced effects. In oceans, changes in local carbon depended upon modified temperature and atmospheric CO_2 level as well as three-dimensional circulation. Although more comparisons with empirical data are warranted, a previous study also concluded that FEA-caused cooling can increase carbon storage in tropical forests (Doughty *et al* 2010).

Some previous studies on the impact of anthropogenic (Mercado *et al* 2009) or fire (Rap *et al* 2015)

aerosols on land carbon neglected aerosol-induced temperature changes, so they could not capture all the effects reported above. Conversely, we neglected the aerosol-induced increase in diffuse radiation that these previous studies addressed. Had we also included this diffuse radiation effect, our spatial patterns of land carbon changes would likely have remained similar but with results shifted towards more positive values. For most of Latin America, westernmost Africa, and equatorial Asia, FEA-caused increases in land carbon storage would therefore have been higher. We hypothesize that FEA would still have reduced land carbon in central Africa, albeit less than simulated here, because the large decrease in surface radiation (e.g. figure 1(*b*)) would have had a stronger impact than the corresponding increase in diffuse radiation, as suggested by the curvilinear relationship between productivity and diffuse fraction (Knohl and Baldocchi 2008) or FEA amount (Rap *et al* 2015) reported for other regions.

Effects on local carbon stocks became much stronger when FEA forcing acted over many centuries vs. 30 years (figure 3(*c*) vs. 2(*b*)), yet the global changes remained small (table 2) due to offsetting increases and decreases. Even if limited, FEA impacts on global carbon stocks should not be considered negligible: the mean FEA-caused decrease of atmospheric CO_2 over 1991–2020 was almost 12 ppmv under TR-1170-MAX, for which our ERF results (preindustrial and present-day global mean values of −0.38 and −0.25 W m^{-2}, respectively) were realistic. FEA forcing and its impacts might also increase in the future if fires become more frequent, but we stress that: (1) a larger FEA forcing did not always led to larger changes in global carbon stocks (table 2); and (2) for a given amount of FEA, the exact forcing also depends upon anthropogenic aerosol emissions.

We can also compare our results with the effect of fire itself on carbon stocks. We took the year-1750 'CO_2 only' equilibrium from Landry *et al* (2015), which did not account for FEA forcing, and continued the equilibrium simulation for 10000 years after suddenly switching off the fire module and letting all carbon pools evolve freely. The net effect of fire was to decrease land carbon stocks by 161 Pg C, which increased ocean and atmosphere carbon stocks by 129 and 33 Pg C, respectively. This corresponds to mean changes of about −1050 g C m^{-2} over land and +360 g C m^{-2} over ocean. By comparison, FEA-caused local changes in carbon stocks for the year-1850 equilibrium had an absolute value ≥200 g C m^{-2} over 2%, 13%, and 32% of all grid cells for MIN, BG, and MAX, respectively (present-day values for multi-century FEA forcing (figures S5(*c*), 3(*c*), and S6(*c*)) were very similar).

4.2. Remote effects and feedbacks

We found consequential FEA remote effects acting on the carbon cycle over decadal timescales for at least two regions. Due to prevailing westward winds, the strong negative ERF west of central Africa (figure 1(*a*)) contributed to the FEA-induced cooling over eastern South America (figures 2(*a*) and 3(*b*)). Vegetation productivity in the region benefited from this African-originating cooling, especially as the reduction in surface radiation was much less severe than for central Africa (figure 1(*b*)). Slower decomposition of soil–litter, to which the African-originating cooling also contributed, then compounded the effect of enhanced vegetation productivity, resulting in relatively high carbon increases in the region (figures 2(*b*) and 3(*c*)). Due to prevailing northwestward winds over northern Australia, a similar remote effect generally increased land carbon in equatorial Asia. These remote effects are possibly strengthened by fire-caused exports of nitrogen (Chen *et al* 2010) and other nutrients transported by the same prevailing winds; these exports were not considered in our study.

Our results indicate another potential FEA remote effect on the carbon cycle on much longer timescales. Negative ERF due to FEA predominantly occurred in tropical regions (figure 1(*a*)), yet on centennial timescales the resulting global cooling increased sea ice cover, especially in the Arctic, which further cooled the global climate (temperature trend in figure 3(*a*)) and substantially decreased high-latitude temperatures (figures 3(*b*) vs. 2(*a*)). As a result, carbon stocks decreased in boreal forests due to cooling-induced productivity reduction and probably increased in oceans due to cooling-induced effect on CO_2 solubility.

Although we did not address this question with fully prognostic and transient simulations, our simplified assessment seemed to go against the existence of strong regional-scale positive FEA–carbon cycle feedbacks, except possibly for the highest FEA amount considered. Even if potential positive feedbacks between FEA and the carbon cycle appeared small based on the effects studied here (i.e. FEA-caused changes in temperature and surface radiation), meaningful positive feedbacks could arise through other processes like FEA-induced decreases in precipitation over tropical regions (Tosca *et al* 2013, 2015).

4.3. Modelling insights

Previous studies including aerosol–cloud interactions obtained present-day FEA-caused global mean ERF between −1.5 W m^{-2} (Ward *et al* 2012) and +0.9 W m^{-2} (Jacobson 2014). Even if excluding these two extreme results, recent studies differ by ∼1 W m^{-2}. These discrepancies stem from the still relatively low level of scientific understanding for aerosol–cloud interactions (Myhre *et al* 2013), which represent the main uncertainty when modelling long-term FEA forcing over large spatial scales. FEA amounts and episodicity appear as smaller uncertainty sources. For the TR-30-X simulations, we found a range of

0.22 W m^{-2} for global mean ERF between MIN and MAX, which likely bounded the range of plausible FEA amounts. A study on the episodicity of FEA in a model giving much more negative ERF than ECHAM-HAMMOZ found a global mean ERF difference of 0.2 W m^{-2} between emissions interpolated from monthly mean values vs. emissions that accounted for the number of fire days and fire events each month (Clark *et al* 2015). Simple vs. parameterized FEA emission heights (Veira *et al* 2015) as well as the nudging meteorology and the potential FEA–carbon cycle feedback assessed here appear as even smaller effects, modifying global mean ERF by about 0.04, 0.05, and 0.01 W m^{-2}, respectively. However, nudging itself and the set of variables used for it might have an effect comparable to FEA amounts and episodicity (Zhang *et al* 2014).

Modelling FEA effects on the carbon cycle is challenging, because aerosol–climate models are computationally demanding whereas temperature–carbon feedbacks evolve over multi-century timescales. The limited impacts on our results of nudging meteorology as well as feedbacks between FEA forcing and magnitude of FEA suggest that fully online and transient simulations of FEA–carbon interactions might not be necessary to capture first-order effects over long timescales. The major differences between figures 2 and 3, however, highlight the importance of accounting for the existence of FEA forcing over the past centuries and beyond. Due to non-linear interactions between FEA and anthropogenic aerosols (Spracklen and Rap 2013), modellers should ideally use FEA forcing representative of preindustrial atmospheric conditions for equilibrium; given the other uncertainties involved, updating FEA forcing each decade might then be sufficient for transient simulations. Due to seasonal variations in vegetation productivity and sign changes in FEA forcing at the same location during the year, using monthly-variable FEA forcing fields as we did here seems advisable.

4.4. Study limitations

ECHAM-HAMMOZ does not account for brown carbon, which is the fraction of OC that absorbs radiation and therefore warms the climate. Effects of brown carbon are only starting to be represented in aerosol–climate models and remain highly uncertain (Jacobson 2014, Saleh *et al* 2015, Jo *et al* 2016). Our results also excluded the warming caused by BC deposition on snow. Although very small globally, this warming is consequential for climate-related processes in snow-covered regions (Flanner *et al* 2007, Jiang *et al* 2016) and might have reversed the FEA-caused cooling we found around the Arctic (figure 3(b)). In addition to FEA impacts on diffuse radiation and nutrient redistribution discussed above, we neglected nitrate FEA (Akagi *et al* 2011) and biogenic secondary organic aerosols (Scott *et al* 2014), and our modelling framework did not allow to fully capture the effects of FEA-caused precipitation changes (Tosca *et al* 2013, 2015). By prescribing monthly burned area based on 2001–2012 data, we also missed the large fire years of 1997 and 1998, which might be consequential for equatorial Asia (van der Werf *et al* 2010); furthermore, this approach did not account for the regional-scale variations in fire frequency over the past centuries (Marlon *et al* 2013). Although each fire event in the UVic ESCM led to bare ground available for colonization by the different PFTs, these fire-created patches were not subsequently tracked on an individual basis, thereby neglecting the effects of the resulting 'subgrid cell dynamic heterogeneity' (Landry *et al* 2016). Finally, future studies separating the carbon cycle effects due to FEA-caused forcing at the top of the atmosphere vs. at the surface could provide additional insights.

4. Conclusion

We combined an aerosol–climate model and a coupled climate–carbon model to assess FEA forcing effects on carbon cycling over decadal and multi-century timescales. FEA-caused changes in both temperature and surface radiation affected land and ocean carbon stocks, even under the minimum estimate of FEA amounts for which forcing values were much smaller than in previous studies. On decadal timescales, FEA forcing—which had present-day best guess (minimum to maximum) values of −0.10 (−0.03 to −0.25) and −1.3 (−0.4 to −2.3) W m^{-2} at the top of the atmosphere and surface, respectively—directly altered vegetation productivity and soil–litter decomposition, modifying global land, atmosphere, and ocean carbon stocks by <2 Pg C each under all FEA amounts. On a multi-century timescale, FEA-induced cooling increased sea ice cover, further affecting temperature and carbon exchanges. Regional carbon increases and decreases offset each other on land and in oceans, explaining why changes in global stocks remained small (<6 Pg C each under all FEA amounts) even for multi-century FEA forcing. We also found remote effects of FEA-caused cooling from fire in Africa and northern Australia on carbon stocks in eastern South America and equatorial Asia, respectively. The existence of strong regional-scale positive feedbacks between FEA and the carbon cycle was not supported by the simple assessment we performed. We finally emphasize that, contrary to anthropogenic aerosols, consequential amounts of FEA have been affecting the carbon cycle and climate for millions of years. Given that fire activity has been changing through time and that the carbon cycle can take many centuries to respond to a given level of FEA forcing, a long-term perspective on FEA–carbon interactions seems warranted.

Acknowledgments

J-S Landry was funded by a Postdoctoral Fellowship from the Concordia Institute for Water, Energy and Sustainable Systems. A-I Partanen was funded by the Emil Aaltonen Foundation. ECHAM-HAMMOZ is developed by a consortium composed of ETH Zürich, the Max Planck Insitut für Meteorologie (Hamburg), Forschungszentrum Jülich, the University of Oxford, and the Finnish Meteorological Institute, and is managed by the Center for Climate Systems Modeling (C2SM) at ETH Zürich. We also thank the two anonymous reviewers for helping us clarify the manuscript.

References

Akagi S K *et al* 2011 Emission factors for open and domestic biomass burning for use in atmospheric models *Atmos. Chem. Phys.* **11** 4039–72

Andreae M O and Merlet P 2001 Emission of trace gases and aerosols from biomass burning *Glob. Biogeochem. Cycles* **15** 955–66

Chen Y *et al* 2010 Nitrogen deposition in tropical forests from savanna and deforestation fires *Glob. Change Biol.* **16** 2024–38

Clark S K, Ward D S and Mahowald N M 2015 The sensitivity of global climate to the episodicity of fire aerosol emissions *J. Geophys. Res.: Atmos.* **120** 11589–607

Cox P M 2001 Description of the 'TRIFFID' Dynamic Global Vegetation Model. Hadley Centre technical note 24, pp 16 Hadley Centre, Met Office, UK (www.metoffice.gov.uk/media/pdf/9/h/HCTN_24. pdf) (Accessed: 18 April 2016)

Dee D P *et al* 2011 The ERA-Interim reanalysis: configuration and performance of the data assimilation system *Q. J. Roy. Meteor. Soc.* **137** 553–97

Dentener F *et al* 2006 Emissions of primary aerosol and precursor gases in the years 2000 and 1750 prescribed data-sets for *AeroCom Atmos. Chem. Phys.* **6** 4321–44

Doughty C E, Flanner M G and Goulden M L 2010 Effect of smoke on subcanopy shaded light, canopy temperature, and carbon dioxide uptake in an Amazon rainforest *Glob. Biogeochem. Cycles* **24** GB3015

Eby M *et al* 2013 Historical and idealized climate model experiments: an intercomparison of Earth system models of intermediate complexity *Climate of the Past* **9** 1111–40

Eby M *et al* 2009 Lifetime of anthropogenic climate change: Millennial time scales of potential CO_2 and surface temperature perturbations *J. Clim.* **22** 2501–11

Ewen T L, Weaver A J and Eby M 2004 Sensitivity of the inorganic ocean carbon cycle to future climate warming in the UVic coupled model *Atmos. Ocean.* **42** 23–42

Flanner M G, Zender C S, Randerson J T and Rasch P J 2007 Present-day climate forcing and response from black carbon in snow *J. Geophys. Res.* **112** D11202

GFED4, 2014 Global Fire Emission Database (GFED) version 4. (www.globalfiredata.org/) (Accessed: 20 January 2016)

Giglio L, Randerson J T and van der Werf G R 2013 Analysis of daily, monthly, and annual burned area using the fourth-generation global fire emissions database (GFED4) *J. Geophys. Res.* **118** 317–28

Guieu C, Bonnet S Wagener T and Loÿe-Pilot M-D 2005 Biomass burning as a source of dissolved iron to the open ocean? *Geophys. Res. Lett.* **32** L19608

Jacobson M Z 2004 The short-term cooling but long-term global warming due to biomass burning. *J. Clim.* **17** 2909–26

Jacobson, M Z 2014 Effect of biomass burning on climate, accounting for heat and moisture fluxes, black and brown carbon, and cloud absorption effects. *J. Geophys. Res.: Atmos.* **119** 8980–9002

Jiang Y *et al* 2016 Impacts of global open-fire aerosols on direct radiative, cloud and surface-albedo effects simulated with CAM5. *Atmos. Chem. Phys.* **16** 14805–24

Jo D S, Park R J, Lee S, Kim S-W and Zhang X 2016 A global simulation of brown carbon: implications for photochemistry and direct radiative effect *Atmos. Chem. Phys.* **16** 3413–32

Johnston F A *et al* 2012 Estimated global mortality attributable to smoke from landscape fires. *Environ. Health Perspect* **120** 695–701

Jones A, Haywood J M and Boucher O 2007 Aerosol forcing, climate response and climate sensitivity in the Hadley Centre climate model *J. Geophys. Res.* **112** D20211

Kaiser J W *et al* 2012 Biomass burning emissions estimated with a global fire assimilation system based on observed fire radiative power *Biogeosciences* **9** 527–54

Knohl A and Baldocchi D D 2008 Effects of diffuse radiation on canopy gas exchange processes in a forest ecosystem. *J. Geophys. Res.* **113** G02023

Landry J-S and Matthews H D 2016 Non-deforestation fire vs. fossil fuel combustion: the source of CO_2 emissions affects the global carbon cycle and climate responses. *Biogeosciences* **13** 2137–49

Landry J-S, Matthews H D and Ramankutty N 2015 A global assessment of the carbon cycle and temperature responses to major changes in future fire regime *Clim Change* **133** 179–92

Landry J-S, Ramankutty N and Parrott L 2016 Investigating the effects of subgrid cell dynamic heterogeneity on the large-scale modelling of albedo in boreal forests *Earth Interactions* **20** 1–23

Lin H and Leaitch W 1997 Development of an in-cloud aerosol activation parameterization for climate modelling. In: *Proc. of the WMO Workshop on Measurement of Cloud Properties for Forecasts of Weather, Air Quality and Climate* (Geneva: World Meteorological Organization) pp 328–35

Lohmann U, Feichter J, Chuang C C and Penner J E 1999 Prediction of number of cloud droplets in the ECHAM GCM *J. Geophys. Res.* **104** 9169–98

Lohmann U *et al* 2007 Cloud microphysics and aerosol indirect effects in the global climate model ECHAM5-HAM *Atmos. Chem. Phys.* **7** 3425–46

Mahowald N 2011 Aerosol indirect effect on biogeochemical cycles and climate *Science* **334** 794–6

Mahowald N *et al* 2011 Aerosol impacts on climate and biogeochemistry *Annu. Rev. Env. Resour.* **36** 45–74

Mahowald N M *et al* 2005 Impacts of biomass burning emissions and land use change on Amazonian atmospheric phosphorus cycling and deposition *Glob. Biogeochem. Cycles* **19** GB4030

Marlon J R *et al* 2013 Global biomass burning: a synthesis and review of Holocene paleofire records and their controls *Quaternary Sci. Rev.* **65** 5–25

Matthews, H D, Eby M, Ewen T, Friedlingstein P and Hawkins B J 2007 What determines the magnitude of carbon cycle-climate feedbacks? *Glob. Biogeochem. Cycles* **21** GB2012

Matthews H D, Weaver A J, Meissner K J, Gillett N P and Eby M 2004 Natural and anthropogenic climate change: incorporating historical land cover change, vegetation dynamics and the global carbon cycle *Clim. Dynam.* **22** 461–79

Meissner K J, Weaver A J, Matthews H D and Cox P M 2003 The role of land surface dynamics in glacial inception: a study with the UVic Earth System Model *Clim. Dynam.* **21** 515–37

Mercado L M *et al* 2009 Impact of changes in diffuse radiation on the global land carbon sink. *Nature* **458** 1014–7

Myhre G *et al* 2013 Anthropogenic and natural radiative forcing *Climate Change 2013: The Physical Basis. Contribution of Working Group I to the Fifth Assessment Report of the International Panel on Climate Change* ed T F Stocker *et al* (Cambridge, UK: Cambridge University Press) pp 659–740

Rap A *et al* 2013 Natural aerosol direct and indirect radiative effects *Geophys. Res. Lett.* **40** 3297–301

Rap A *et al* 2015 Fires increase Amazon forest productivity through increases in diffuse radiation *Geophys. Res. Lett.* **42** 4654–62

Saleh R *et al* 2015 Contribution of brown carbon and lensing to the direct radiative effect of carbonaceous aerosols from biomass and biofuel burning emissions *J. Geophys. Res.: Atmos.* **120** 10285–96

Schmittner A, Oschlies A, Matthews H D, Galbraith E D 2008 Future changes in climate, ocean circulation, ecosystems, and biogeochemical cycling simulated for a business-as-usual CO_2 emission scenario until year 4000 AD *Glob. Biogeochem. Cycles* **22** GB1013

Scott C E *et al* 2014 The direct and indirect radiative effects of biogenic secondary organic aerosol *Atmos. Chem. Phys.* **14** 447–70

Spracklen D V and Rap A 2013 Natural aerosol–climate feedbacks suppressed by anthropogenic aerosol *Geophys. Res. Lett.* **40** 5316–9

Steiner A L and Chameides W L 2005 Aerosol-induced thermal effects increase modelled terrestrial photosynthesis and transpiration *Tellus* **57B** 404–11

Stevens B *et al* 2013 Atmospheric component of the MPI-M Earth System Model: ECHAM6 *J. Adv. Model Earth Sy.* **5** 146–72

Tosca M G, Diner D J, Garay M J and Kalashnikova O V 2015 Human-caused fires limit convection in tropical Africa: first temporal observations and attribution *Geophys. Res. Lett.* **42** 6492–501

Tosca M G, Randerson J T and Zender C S 2013 Global impact of smoke aerosols from landscape fires on climate and the Hadley circulation *Atmos. Chem. Phys.* **13** 5227–41

Unger N *et al* 2010 Attribution of climate forcing to economic sectors *Proc. Natl Acad. Sci.* **107** 3382–87

van der Werf G R *et al* 2010 Global fire emissions and the contribution of deforestation, savanna, forest, agricultural, and peat fires (1997–2009) *Atmos. Chem. Phys.* **10** 11707–35

van Vuuren D P *et al* 2011 The representative concentration pathways: an overview *Clim. Change* **109** 5–31

Veira A, Kloster S, Schutgens N A J and Kaiser J W 2015 Fire emission heights in the climate system—Part 2: Impact on transport, black carbon concentrations and radiation *Atmos. Chem. Phys.* **15** 7173–93

Ward D S *et al* 2012 The changing radiative forcing of fires: global model estimates for past, present and future *Atmos. Chem. Phys.* **12** 10857–86

Weaver A J *et al* 2001 The UVic earth system climate model: model description, climatology, and applications to past, present and future climates *Atmos. Ocean* **39** 361–428

Zhang K *et al* 2012 The global aerosol-climate model ECHAM-HAM, version 2: sensitivity to improvements in process representations *Atmos. Chem. Phys.* **12** 8911–49

Zhang K *et al* 2014 Technical Note: On the use of nudging for aerosol–climate model intercomparison studies *Atmos. Chem. Phys.* **14** 8631–45